Measuring Attitude Rates Through Angular Momentum Gyros

Hong-Hua Zhang*
Beijing Institute of Control Engineering, 100080 Beijing, People's Republic of China

Introduction

STABLE attitude pointing is required for some remote sensing satellites to get high-resolution imaging. A sensor for measuring angular rates with high accuracy is necessary for the attitude control system because the accuracy of the angular rates principally determines the stability of the controlled spacecraft. This Note is devoted to the description of a sensor called the angular momentum gyro (AMG).

The usual sensors to measure the angular rates of a spacecraft are rate gyros (RG) and rate-integrating gyros (RIG).[1–4] The spacecraft motion about the gyro's input axis causes the gyro's gimbal supporting the spin axis to precess about the output axis. The angular rates are then determined according to the moment relationship along the gyro's output axis. The closed-loop RIG is an example where the torquer in the output axis generates a moment to balance the gyro torque. The angular rates are determined by counting the number of current pulses to the torquer in a sample period. The accuracy of the closed-loop RIG depends on the current pulse frequency. Increasing the current pulse frequency will increase the accuracy of the closed-loop gyro; however, this action demands improved technology.

The AMG, developed from the control moment gyro (CMG) concept,[5–8] is proposed in this Note to give an alternate approach to improving the accuracy of the closed-loop RIG. The angular momentum of the spacecraft is directly sensed by the AMG according to the moment relationship along the input axis of the gyro. The angular rates are then derived from the momentum, provided that the moments of inertia of the spacecraft are given. For some spacecraft configurations a small angular rate is related to a large angular momentum or a large AMG's gimbal precession angle induced by the angular momentum. Therefore, if the measuring accuracy of the gimbal precession angle is appropriately small, then the AMG is capable of sensing small angular momentum and thus very small angular rates. Therefore, the AMG makes it possible to improve the accuracy of the closed-loop RIG.

Description of a Single-Gimbal AMG

A single-gimbal AMG mounted in the spacecraft is shown in Fig. 1. It has nearly the same components as the closed-loop RIG, which include a rotor, a gimbal supporting the spinning axis, a torquer, and an output sensor. The torquer is used to generate the moment to balance the gyro torque, whereas the sensor is used to measure the precession angle of the gimbal.

The working process of the AMG is as follows: 1) an incoming angular rate about the input axis induces the gyro torque along the output axis, 2) the torquer generates a moment to balance the gyro torque so that the gimbal angle remains near zero and the nominal angular rate is determined according to the current pulses to the torquer, and 3) the angular rate is then determined from the remaining gimbal precession angle and the nominal angular rate according to the moment relationship along the input axis.

Determining the Nominal Angular Rates by AMG

The principle for determining the nominal angular rate by AMG is the same as that by closed-loop RIG and is outlined in this section.

Received 4 January 1999; revision received 22 July 1999; accepted for publication 2 August 1999.

*Senior Engineer, P.O. Box 2729; zhh@public.east.cn.net.

For practical gyros the following assumptions hold: 1) the rotor spins with a constant rate about its axis, 2) the rotor's center of mass is coincident with the gyro system's center of mass, 3) the rotor's spinning angular momentum is considerably greater than its nonspinning angular momentum because of the spin of the gimbal, and 4) the spacecraft's mass is considerably greater than that of the gyro system.

Construct two coordinate frames $o\boldsymbol{e}_1\boldsymbol{e}_2\boldsymbol{e}_3$ and $o'\boldsymbol{e}'_1\boldsymbol{e}'_2\boldsymbol{e}'_3$ as shown in Fig. 1. The frame $o\boldsymbol{e}_1\boldsymbol{e}_2\boldsymbol{e}_3$ is fixed to the spacecraft with o as the spacecraft's mass center and $\boldsymbol{e}_1$, $\boldsymbol{e}_2$, and $\boldsymbol{e}_3$ as unit vectors along the spacecraft's three inertial principal axes, respectively. The frame $o'\boldsymbol{e}'_1\boldsymbol{e}'_2\boldsymbol{e}'_3$ is fixed in the gyro gimbal with o' as the gyro system's mass center and $\boldsymbol{e}'_1$, $\boldsymbol{e}'_2$, and $\boldsymbol{e}'_3$ as the unit vectors along the input axis, the output axis, and the spinning axis, respectively.

Applying Newton's laws to the gyro system yields

$$M_{g1} = (\omega_2 + \dot{\delta})H_s \cos\delta + \{I_{\text{wp1}} \cos\delta[(-\omega_1 \sin\delta - \omega_3 \cos\delta)\dot{\delta} + \dot{\omega}_1 \cos\delta - \dot{\omega}_3 \sin\delta] + I_{\text{wp3}} \sin\delta[(\omega_1 \cos\delta - \omega_3 \sin\delta)\dot{\delta} + \dot{\omega}_1 \sin\delta + \dot{\omega}_3 \cos\delta]\} \tag{1}$$

$$M_{g2} = I_{\text{wp2}}(\dot{\omega}_2 + \ddot{\delta}) + (\omega_3 H_s \sin\delta - \omega_1 H_s \cos\delta) \tag{2}$$

$$M_{g3} = -(\omega_2 + \dot{\delta})H_s \sin\delta + \{I_{\text{wp1}} \sin\delta[(\omega_1 \sin\delta + \omega_3 \cos\delta)\dot{\delta} - \dot{\omega}_1 \cos\delta + \dot{\omega}_3 \sin\delta] + I_{\text{wp3}} \cos\delta[(\omega_1 \cos\delta - \omega_3 \sin\delta)\dot{\delta} + \dot{\omega}_1 \sin\delta + \dot{\omega}_3 \cos\delta]\} \tag{3}$$

where M_{g1}, M_{g2}, and M_{g3} are the components of the torque acting on the gyro along axes $\boldsymbol{e}_1$, $\boldsymbol{e}_2$, and $\boldsymbol{e}_3$, respectively; ω_1, ω_2, and ω_3 are the spacecraft's absolute angular velocity components along axes $\boldsymbol{e}_1$, $\boldsymbol{e}_2$, and $\boldsymbol{e}_3$, respectively; I_{wp1}, I_{wp2}, and I_{wp3} are the gyro's moments of inertia about axes $\boldsymbol{e}'_1$, $\boldsymbol{e}'_2$, and $\boldsymbol{e}'_3$, respectively; δ and $\dot{\delta}$ are the gimbal's rotation angle (precession angle) and the angular rate with respect to the spacecraft, respectively; and H_s is the magnitude of the angular momentum of the rotor along its spinning axis.

Because the gimbal precession angle is small for the closed-loop gyro, the steady-state moment relationship along $\boldsymbol{e}_2$ is derived from Eq. (2) and assumptions 1–4:

$$-\omega_1 H_s = M_{g2} \tag{4}$$

As in the closed-loop RIG, M_{g2} is determined by control torque M_{c2} (which is generated by the torquer) and satisfies $\omega_1 H_s = M_{c2}$. The torque M_{c2} drives the gimbal precession angle to its original position in steady state.

Denote the sample period for the angular rate by T_s and the current pulse period to the torquer by T_q. Suppose that one sample period contains N pulses (periods), i.e., $T_s = NT_q$; the largest angular rate $\omega_{1\,\max}$ corresponds to N (all positive or all negative) pulses in one sample period. If there are n pure pulses (the difference between

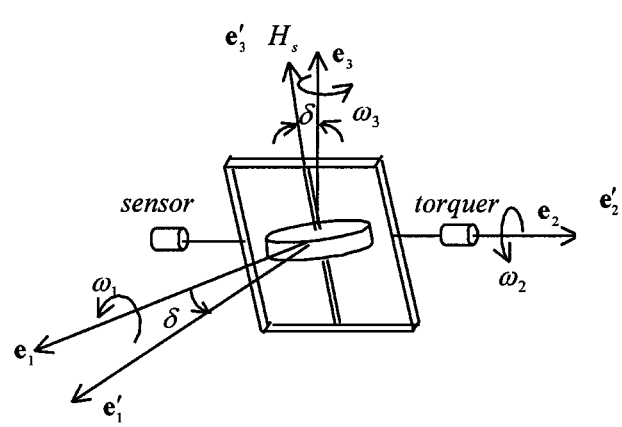

Fig. 1 Single-gimbal AMG.

the number of negative and positive pulses) in one sample period, the nominal angular rate $\omega_{1\,\mathrm{nom}}(t)$ at time t will be determined by

$$\omega_{1\,\mathrm{nom}}(t) = (n/N)\omega_{1\,\max} = n(\omega_{1\,\max}/f_q)f_s \tag{5}$$

where $f_s = 1/T_s$ is the sample frequency, $f_q = 1/T_q$ is the pulse frequency, and the rotation angle for one pulse is denoted by $\omega_{1\,\max}/f_q$.

Obviously, the nominal angular rate $\omega_{1\,\mathrm{nom}}(t)$ is not necessarily equal to the real angular rate $\omega_1(t)$. The supreme difference between the nominal angular rate and the real angular rate is

$$\omega_{1\,\min} = (\omega_{1\,\max}/f_q)f_s \tag{6}$$

This difference causes gimbal-angle departure from the zero position.

According to the sampling theorem, the sample period should be large enough to reconstruct the real (attitude rate) signal. One option to improve the accuracy is to minimize $\omega_{1\,\max}/f_q$, which is, however, very difficult in practice. An alternate choice to improve the accuracy is through measuring the gimbal angle, which will be described in the next section.

Determining the Angular Rate by AMG

Denote the spacecraft's moments of inertia about axes $\boldsymbol{e}_1$, $\boldsymbol{e}_2$, and $\boldsymbol{e}_3$ by I_1, I_2, and I_3, respectively. Newton's laws applied to the spacecraft yield

$$I_1\dot{\omega}_1 - (I_2 - I_3)\omega_2\omega_3 = T_1 - M_{g1} \tag{7}$$

$$I_2\dot{\omega}_2 - (I_3 - I_1)\omega_3\omega_1 = T_2 - M_{g2} \tag{8}$$

$$I_3\dot{\omega}_3 - (I_1 - I_2)\omega_1\omega_2 = T_3 - M_{g3} \tag{9}$$

where T_1, T_2, and T_3 are the external torques acting on the spacecraft and $-M_{g1}$, $-M_{g2}$, and $-M_{g3}$ are the torques generated by gyros.

The moment relationship along the axis $\boldsymbol{e}_1$ is derived from Eqs. (1) and (7):

$$\begin{aligned} I_1\dot{\omega}_1 - (I_2 - I_3)\omega_2\omega_3 &= T_1 - (\omega_2 + \dot{\delta})H_s\cos\delta \\ &\quad - \{I_{\mathrm{wp1}}\cos\delta[(-\omega_1\sin\delta - \omega_3\cos\delta)\dot{\delta} + \dot{\omega}_1\cos\delta - \dot{\omega}_3\sin\delta] \\ &\quad + I_{\mathrm{wp3}}\sin\delta[(\omega_1\cos\delta - \omega_3\sin\delta)\dot{\delta} + \dot{\omega}_1\sin\delta + \dot{\omega}_3\cos\delta]\} \end{aligned} \tag{10}$$

Omitting the last term in Eq. (10) by assumptions 3 and 4 yields

$$I_1\dot{\omega}_1 - (I_2 - I_3)\omega_2\omega_3 = T_1 - \omega_2 H_s\cos\delta - H_s\dot{\delta}\cos\delta \tag{11}$$

Integrating Eq. (11) over a sample period $[t - T_s, t]$ gives

$$\begin{aligned} I_1\omega_1(t) + H_s\sin\delta(t) &= I_1\omega_1(t - T_s) + H_s\sin\delta(t - T_s) \\ &\quad + \int_{t-T_s}^{t} T_1(\upsilon)\,\mathrm{d}\upsilon + \int_{t-T_s}^{t} (I_2 - I_3)\omega_2(\upsilon)\omega_3(\upsilon)\,\mathrm{d}\upsilon \\ &\quad - \int_{t-T_s}^{t} \omega_2(\upsilon)H_s\cos\delta(\upsilon)\,\mathrm{d}\upsilon \end{aligned} \tag{12}$$

Because the gimbal angle $\delta(t)$ is small, it follows from Eq. (12) that

$$\begin{aligned} I_1\omega_1(t) + H_s\delta(t) &= I_1\omega_1(t - T_s) + H_s\delta(t - T_s) \\ &\quad + \int_{t-T_s}^{t} T_1(\upsilon)\,\mathrm{d}\upsilon + \int_{t-T_s}^{t} (I_2 - I_3)\omega_2(\upsilon)\omega_3(\upsilon)\,\mathrm{d}\upsilon \\ &\quad - \int_{t-T_s}^{t} \omega_2(\upsilon)H_s\delta\,\mathrm{d}\upsilon \end{aligned} \tag{13}$$

Equation (13) shows the angular momentum relationship along the input axis, which is independent of the torque on the output axis.

As stated in the preceding section, the torquer on the output axis will make the gimbal angle $\delta(t)$ return to its last position $\delta(t - T_s)$ in steady state if the angular rate $\omega_1(t)$ along the input axis is equal to the nominal angular rate $\omega_{1\,\mathrm{nom}}(t)$ given in Eq. (5), i.e.,

$$\delta(t) = \delta(t - T_s), \qquad \text{if} \qquad \omega_1(t) = \omega_{1\,\mathrm{nom}}(t) \tag{14}$$

Substituting Eq. (14) into Eq. (13) gives

$$\begin{aligned} &I_1\omega_1(t - T_s) + \int_{t-T_s}^{t} T_1(\upsilon)\,\mathrm{d}\upsilon + \int_{t-T_s}^{t} (I_2 - I_3)\omega_2(\upsilon)\omega_3(\upsilon)\,\mathrm{d}\upsilon \\ &\quad - \int_{t-T_s}^{t} \omega_2(\upsilon)H_s\delta\,\mathrm{d}\upsilon = I_1\omega_{1\,\mathrm{nom}}(t) \end{aligned} \tag{15}$$

It follows from Eqs. (12) and (15) that

$$\omega_1(t) = \omega_{1\,\mathrm{nom}}(t) - (H_s/I_1)[\delta(t) - \delta(t - T_s)] \tag{16}$$

Obviously, the spacecraft's moment of inertia should be determined a priori for the AMG. For spacecraft operating in near-polar orbits with the solar arrays fixed to the main body, the moment of inertia can be easily determined. For spacecraft with complex configurations, on-orbit identification techniques can be necessary to estimate the moment of inertia. However, the accuracy of the moment of inertia might not be crucial for the AMG because the sensitivity of the angular rate with respect to the change of the moment of inertia is small if the spacecraft's moment of inertia is large.

AMGs for Three Axes

Measuring the angular velocity components in three axes by AMGs will be described in this section. The AMGs are mounted in the spacecraft with the configuration shown in Fig. 2. One AMG is mounted on each axis ($\boldsymbol{e}_1, \boldsymbol{e}_2, \boldsymbol{e}_3$). Each of the three AMGs is of the same components as that in Fig. 1. Let δ_z, δ_x, and δ_y denote the gimbal precession angles of the gyros with angular momentum H_{sz}, H_{sx}, and H_{sy}, respectively. Then by use of the same method as in the preceding two sections, one can see that

$$\begin{aligned} I_1\dot{\omega}_1 - (I_2 - I_3)\omega_2\omega_3 &= -(\omega_2 + \dot{\delta}_x)H_{sx}\cos\delta + T_1 \\ &\quad + (\omega_3 + \dot{\delta}_y)H_{sy}\sin\delta_y - H_{sz}\omega_{3\,\mathrm{nom}}(t) \end{aligned} \tag{17}$$

$$\begin{aligned} I_2\dot{\omega}_2 - (I_3 - I_1)\omega_3\omega_1 &= -(\omega_3 + \dot{\delta}_y)H_{sy}\cos\delta + T_2 \\ &\quad + (\omega_1 + \dot{\delta}_z)H_{sz}\sin\delta_z - H_{sx}\omega_{1\,\mathrm{nom}}(t) \end{aligned} \tag{18}$$

$$\begin{aligned} I_3\dot{\omega}_3 - (I_1 - I_2)\omega_1\omega_2 &= -(\omega_1 + \dot{\delta}_z)H_{sz}\cos\delta_z + T_3 \\ &\quad + (\omega_2 + \dot{\delta}_x)H_{sx}\sin\delta_x - H_{sy}\omega_{2\,\mathrm{nom}}(t) \end{aligned} \tag{19}$$

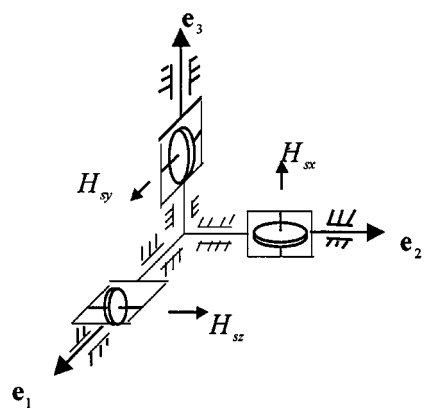

Fig. 2 Three single-gimbal AMGs.

where $\omega_{1\,\mathrm{nom}}(t)$, $\omega_{2\,\mathrm{nom}}(t)$, and $\omega_{3\,\mathrm{nom}}(t)$ are the nominal angular rates, which can be determined by the procedure described by Eq. (5); and $-H_{sz}\omega_{3\,\mathrm{nom}}(t)$, $-H_{sx}\omega_{1\,\mathrm{nom}}(t)$, and $-H_{sy}\omega_{2\,\mathrm{nom}}(t)$ are the reaction torques from the torquers of the gyros. Following the derivation of Eq. (16), the integration of Eqs. (17–19) gives the three angular velocity components:

$$\omega_1(t) = \omega_{1\,\mathrm{nom}}(t) - (H_{sx}/I_1)[\delta_x(t) - \delta_x(t - T_s)] \quad (20)$$

$$\omega_2(t) = \omega_{2\,\mathrm{nom}}(t) - (H_{sy}/I_2)[\delta_y(t) - \delta_y(t - T_s)] \quad (21)$$

$$\omega_3(t) = \omega_{3\,\mathrm{nom}}(t) - (H_{sz}/I_3)[\delta_z(t) - \delta_z(t - T_s)] \quad (22)$$

Accuracy Analysis of the AMG

As indicated in Eq. (16), the output of the AMG satisfies $\delta(t) - \delta(t - T_s) = (-I_1/H_s)[\omega_1(t) - \omega_{1\,\mathrm{nom}}(t)]$. If the ratio I_1/H_s is large, then the minimum angular velocity that the AMG is able to sense may be small, which means that the AMG could improve the accuracy of the usual closed-loop gyro.

Consider an example as follows: The spacecraft's moment of inertia is $I_1 = 10^3$ N-m-s^2. The angular momentum of the gyro is $H_s = 1.05$ N-m-s, the maximum angular rate of the gyro is $\omega_{1\,\max} = 1$ deg/s, and the sample frequency of the gyro is $f_s = 2$ Hz. The pulse frequency of the gyro is $f_q < 2(10^4)$ Hz. (For some gyros $\omega_{1\,\max}/f_q = 0.001$ is a typical value.) Then Eqs. (6) and (16) imply that the closed-loop gyro is not able to sense the angular rate of 10^{-4} deg/s, but the AMG is able to sense the angular rate of 10^{-4} deg/s if the scale error of the gimbal precession angle is 0.1 deg.

Conclusions

The usual closed-loop RIG operates on the moment relationship along the gyro's output axis, and its accuracy depends on the current pulse frequency. The AMG proposed in this Note utilizes the moment relationship along the input axis. It is shown that the AMG directly senses the spacecraft's angular momentum instead of the angular rate through the gimbal precession angle and that the AMG is capable of improving the accuracy of the usual closed-loop gyro provided that the spacecraft's moment of inertia is large.

Acknowledgments

The author would like to thank the editors and the reviewers of this Note for their constructive comments.

References

[1]Shmuel, M., *Aerospace Sensor Systems and Applications*, Springer–Verlag, New York, 1996, pp. 15–200.

[2]Wertz, J. R., *Spacecraft Attitude Determination and Control*, Kluwer Academic, Norwell, MA, 1978, pp. 196–203.

[3]Lawrence, A., *Modern Inertial Technology, Navigation, Guidance, and Control*, Springer–Verlag, New York, 1993, pp. 1–55.

[4]Gary, S. C., Morrow, L. D., and Mamen, R., "Strapdown Navigation Technology: A Literature Survey," *Journal of Guidance and Control*, Vol. 1, No. 3, 1978, pp. 161–172.

[5]Oconnor, B. J., "A Description of the CMG and Its Application to Space Vehicle Control," *Journal of Spacecraft and Rockets*, Vol. 6, No. 3, 1969, pp. 225–231.

[6]Jacot, A. D., "Control Moment Gyros in Attitude Control," *Journal of Spacecraft and Rockets*, Vol. 3, No. 10, 1966, pp. 1313–1320.

[7]Cilburn, B., "Computational Consideration for a Spacecraft Attitude Control System Employing Control Moment Gyros," *Journal of Spacecraft and Rockets*, Vol. 14, No. 1, 1977, pp. 45–53.

[8]Zhang, C., and He, C., *Inertial Technology*, Science Press of China, Beijing, 1987, pp. 31–84.

C. A. Kluever
Associate Editor

Fabrication and Testing of a Leading-Edge-Shaped Heat Pipe

David E. Glass*
Analytical Services and Materials, Inc., Hampton, Virginia 23666
Charles J. Camarda†
NASA Johnson Space Center, Houston, Texas 77058
and
Michael A. Merrigan,§ J. Tom Sena,‡ and Robert S. Reid‡
Los Alamos National Laboratory, Los Alamos, New Mexico 87545

Introduction

STAGNATION regions, such as wing and tail leading edges and nose caps, are critical design areas of hypersonic aerospace vehicles because of the hostile thermal environment those regions experience during flight. As a hypersonic vehicle travels through the Earth's atmosphere, the high local heating and aerodynamic forces cause very high temperatures, severe thermal gradients, and high stresses. Analytical studies and laboratory and wind-tunnel tests indicate that a solution to the thermal–structural problems associated with stagnation regions of hypersonic aerospace vehicles might be obtained by the use of heat pipes to cool these regions.

Preliminary design studies at NASA Langley Research Center (LaRC) indicate that a refractory-composite/refractory-metal heat-pipe-cooled leading edge can reduce the leading-edge mass by over 50% compared to an actively cooled leading edge, can completely eliminate the need for active cooling, and has the potential to provide failsafe and redundant features.[1] Recent work to develop this novel refractory-composite/refractory-metal heat-pipe-cooled leading edge for hypersonic vehicles combines advanced high-temperature materials, coatings, and fabrication techniques with an innovative thermal–structural design. Testing of a component at NASA LaRC with three straight molybdenum–rhenium (Mo–Re) heat pipes embedded in carbon/carbon (C/C) has demonstrated the feasibility of operating heat pipes embedded in C/C (Ref. 2). In those tests, the heat pipes were tested with quartz lamps up to temperatures near 2200°F. Some of the key concepts utilized in the fabrication of the refractory-composite heat-pipe-cooled leading edge, such as a compliant or removable layer to reduce thermal stresses and a slightly convex surface to maintain good thermal contact, have been patented.[3]

The present Note discusses the next step in the development of a refractory-composite/refractory-metal heat-pipe-cooled leading edge: a leading-edge-shaped heat pipe with a relatively sharp leading edge and a thin wall thickness. (More details of this work may be found in Ref. 4.) Numerous fabrication issues were resolved in the fabrication of both the heat-pipe container and wick. The heat pipe was fabricated from arc cast Mo–41Re, used lithium as the working fluid, and had a D-shaped cross section and a 400 × 400 mesh Mo–5Re screen wick with a single artery along the length of the

Received 1 October 1998; revision received 25 February 1999; accepted for publication 25 June 1999.

*Senior Scientist; currently Aerospace Engineer, Mail Stop 396, Metals and Thermal Structures Branch, NASA Langley Research Center, Hampton, VA 23681. Senior Member AIAA.

†Astronaut, Mail Code CB, 2101 NASA Road. Associate Fellow AIAA.

§Retired, P.O. Box 1663, Mail Stop J576; currently Technical Staff Member, Comforce, Inc., Los Alamos, NM 87545.

‡Staff Member, Energy and Process Engineering, P.O. Box 1663, Mail Stop J576.